Research Article | Vol. 27, No. 19 / 16 September 2019 / Optics Express 27191

Optics EXPRESS

Pure phase modulation based on a silicon plasma dispersion modulator

HONG DENG[1,2,*] AND WIM BOGAERTS[1,2]

[1] Photonics Research Group, Ghent University - imec, Department of Information Technology,Technologiepark-Zwijnaarde 126, 9052 Gent, Belgium
[2] Center for Nano and Biophotonics (NB-Photonics), Ghent University, Ghent, Belgium
[*] hong.deng@ugent.be

Abstract: Plasma dispersion modulators (PDMs), such as carrier injection modulators and carrier depletion modulators, are widely used for high speed phase modulation in silicon photonic circuits, but they suffer from spurious intensity modulation. This can be a problem in coherent communication systems that make use of complex multi-level quadrature modulation formats, as well as analog applications such as microwave photonics. In this article, a method to achieve pure phase modulation using PDMs is proposed based on a configurable modulator circuit. The configurable modulator is implemented as a Mach-Zehnder interferometer with a PDM and tunable couplers (TCs). The spurious intensity modulation of the phase modulated lightwave can be compensated by tuning the coupling ratios of the TCs and the phase delay between the two arms of the MZI. Simulation results show that for a depletion modulator, the 1.26 dB spurious intensity modulation can be suppressed down to 0.023 dB within a phase range of 0.4π, and for injection modulator, the 1.27 dB spurious intensity modulation can be suppressed down to 0.07 dB within a phase range of 0.76π.

1. Introduction

Silicon photonic circuits are becoming ever more popular in recent years, for various applications in data communication, optical sensing, and microwave photonics [1–4]. In many of these applications, electro-optical modulators play an important role. Plasma dispersion modulators (PDMs), implemented by embedding a P(I)N junction into a silicon waveguide, are the most commonly used solution for high speed optical phase modulation, and the phase modulation can be easily converted to intensity modulation by using interferometric circuits, such as Mach - Zehnder interferometers (MZIs) and microring resonators [5,6]. In other material systems, phase modulators based on the Pockels effect are preferred, but this effect is not present in silicon. Therefore, the preferred phase modulation mechanisms is based on free carriers.

The refractive index in silicon waveguides depends on the density of free carriers, which is commonly known as the plasma dispersion effect [7]. By removing or injecting the free carriers in a silicon waveguide core, a PDM can change the refractive index of the waveguide and induce a phase shift in the guided light, implementing a carrier depletion modulator or a carrier injection modulator. The change of the refraction index at 1550 nm can be described as [8]:

$$\Delta n = -5.4 \times 10^{-22} \Delta N^{1.011} - 1.53 \times 10^{-18} \Delta P^{0.838} \tag{1}$$

where ΔN and ΔP are the carrier densities of electrons and holes [cm^{-3}]. However, the change in carrier density also leads to the change in absorption of the waveguide, which can be described as [8]:

$$\Delta \alpha = 8.88 \times 10^{-21} \Delta N^{1.167} + 5.84 \times 10^{-20} \Delta P^{1.109} \tag{2}$$

Figure 1 shows the measured direct current responses for a carrier depletion modulator and an injection modulator [9]. As can be seen, the variation in the absorption is not negligible, leading

#370613 https://doi.org/10.1364/OE.27.027191
Journal © 2019 Received 21 Jun 2019; revised 21 Aug 2019; accepted 24 Aug 2019; published 12 Sep 2019

Optics EXPRESS

to a spurious intensity modulation. In many applications, the introduced intensity distortion can degenerate the system performance, especially in communication systems based on complex higher-order modulation formats.

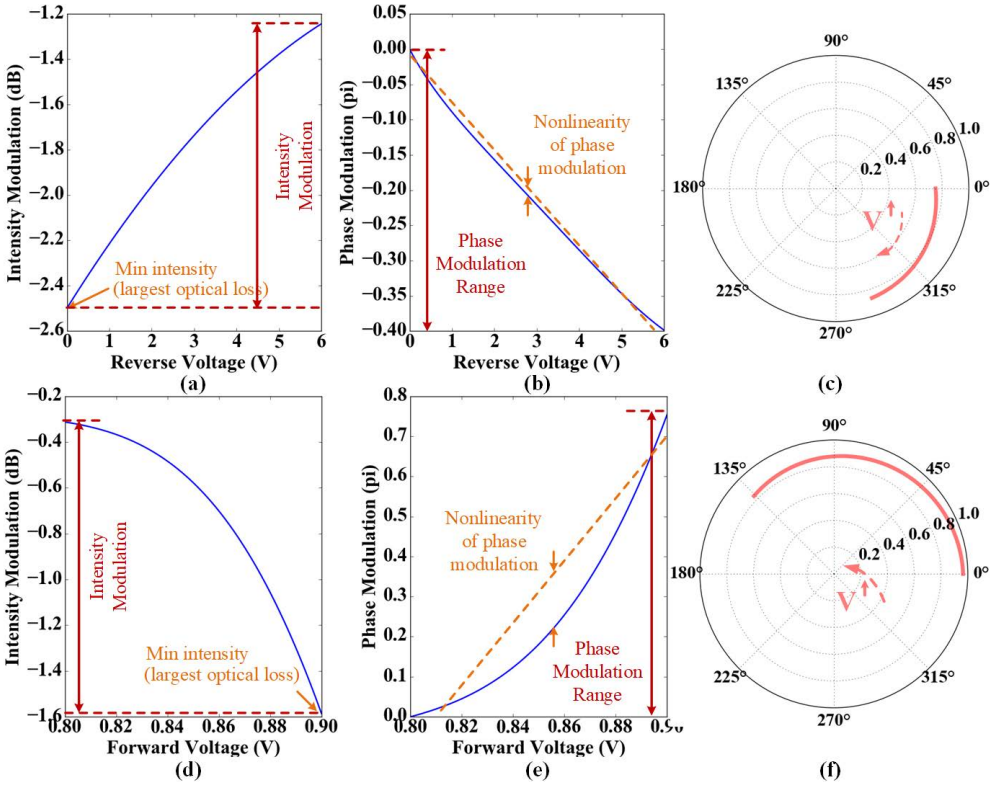

Fig. 1. (a) Measured intensity modulation and (b) phase modulation response of the used depletion modulator model (0 V to 6 V) [9]; (c) modulation curve of the depletion modulator in polar diagram (0 V to 6 V);(d) Measured intensity modulation and (e) phase modulation response of the used injection modulator model (0.8 V to 0.96 V); (f) modulation curve of the injection modulator in polar diagram (0.8 V to 0.9 V);

To realize a pure phase modulation in a silicon photonics platform one can use the thermal effect or introduce new materials with a strong electro-optic effect. In [10], a silicon-organic hybrid modulator is used to implement a pure phase modulation, and demonstrated a 16QAM system at 112 Gbit/s with a BER of 5.1×10^{-5}. However, this silicon organic hybrid integration is not compatible with all silicon photonics platforms. In [11], a thermo-optic phase shifter was used with no extra absorption, but its modulation bandwidth is limited to a few MHz.

In recent years, PDMs were utilized in numerous structures and applications, and in several analysis papers the spurious intensity modulation was discussed [9,12–14]. However, there has been no discussion on compensating this spurious intensity modulation. In this article, we report a method to compensate the spurious intensity modulation of a PDM, by embedding it to a configurable modulator circuit. The method is valid for both depletion and injection modulators, and can be applied in any silicon photonics platform with modulator building blocks. Simulation results show that a 1.26 dB depletion modulator induced spurious intensity modulation can be suppressed down to 0.02 dB within a phase range of 0.4π, and a 1.27 dB injection modulator introduced intensity modulation can be reduced to 0.07dB within a phase range of 0.4π. Furthermore, the circuit can be used to optimize other performance metrics, such

Optics EXPRESS

as the overall insertion loss, phase modulation range and linearity of the phase modulation, which are also indicated in Fig. 1. The technique does not change the modulator element itself. Instead, it is embedded into a small optical circuit that compensates for the nonidealities in the modulator response. As such, it can be applied to existing platforms and standard building blocks from a process design kit (PDK), even if the internal details of the building blocks are not available.

The paper is organized as follows: In Section 2, we show the structure of the proposed configurable modulator and elaborate the principle for suppressing spurious intensity modulation of a PDM; In Section 3, models for depletion and injection modulators are built and simulation results are elaborated. A conclusion is made in Section 4.

2. Principle

The proposed configurable modulator circuit is an MZI structure consisting of two tunable couplers (TCs), a PDM and a phase shifter, as shown in Fig. 2. The phase shifters can be implemented by silicon heaters [15] or liquid crystal infiltration [16]. The PDM in one arm is used to introduce a phase modulation, and the phase shifter in the other arm adjusts the phase delay between the two arms. The TCs are utilized to tune the relative intensity of the light fed into the two arms, which is realized by tuning the phase shifters in the MZI splitter/combiner with 50:50 directional couplers [17].

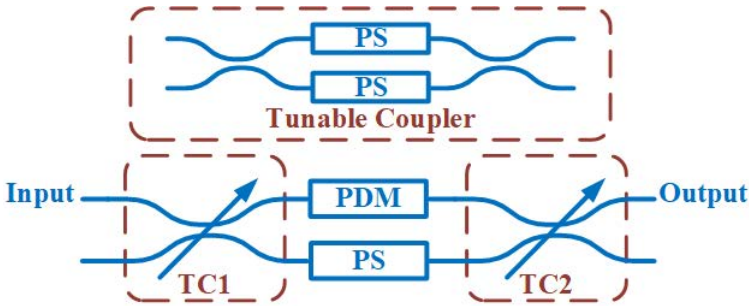

Fig. 2. Schematic of the proposed configurable modulator. PS: phase shifter; PDM: plasma dispersion modulator; TC: tunable coupler.

Because the phase difference between the two arms of the MZI can be fully tuned by the phase shifters [15], the precise phase response of the TCs is not relevant. The transformation matrix of TC can be described as:

$$\begin{bmatrix} E_{c1} \\ E_{c2} \end{bmatrix} = \begin{bmatrix} \sqrt{(1-\kappa)} & j\sqrt{\kappa} \\ j\sqrt{\kappa} & \sqrt{(1-\kappa)} \end{bmatrix} \times \begin{bmatrix} E_{c3} \\ E_{c4} \end{bmatrix} \tag{3}$$

where E_{c1} and E_{c2} are the complex amplitude of the TC's outputs' modes, E_{c3} and E_{c4} are the complex amplitude of inputs' modes, and κ is the splitting ratio of the TC.

Meanwhile, the transformation matrix of both MZI arms can be expressed as:

$$\begin{bmatrix} E_{a1} \\ E_{a2} \end{bmatrix} = \begin{bmatrix} \alpha(V)e^{-j\phi_m(V)} & 0 \\ 0 & e^{(-j\phi_s)} \end{bmatrix} \times \begin{bmatrix} E_{a3} \\ E_{a4} \end{bmatrix} \tag{4}$$

where E_{a1} and E_{a3} are the output field and input of the PDM arm, E_{a2} and E_{a4} are the output and input of the phase shifter arm, $\alpha(V)$ and $\phi_m(V)$ are the intensity and phase response of the PDM, and ϕ_s is the phase response of the phase shifter.

Optics EXPRESS

Thus, the transformation matrix of the proposed configurable modulator can be calculated as:

$$\begin{aligned}\begin{bmatrix}E_{out1}\\E_{out2}\end{bmatrix} &= \begin{bmatrix}\sqrt{(1-\kappa_2)} & j\sqrt{\kappa_2}\\ j\sqrt{\kappa_2} & \sqrt{(1-\kappa_2)}\end{bmatrix}\times\begin{bmatrix}\alpha(V)e^{-j\phi_m(V)} & 0\\ 0 & e^{-j\phi_s}\end{bmatrix}\times\begin{bmatrix}\sqrt{(1-\kappa_1)} & j\sqrt{\kappa_1}\\ j\sqrt{\kappa_1} & \sqrt{(1-\kappa_1)}\end{bmatrix}\times\begin{bmatrix}E_{in1}\\E_{in2}\end{bmatrix}\\ &= \begin{bmatrix}\sqrt{(1-\kappa_1)(1-\kappa_2)}\alpha(V)e^{-j\phi_m(V)} - \sqrt{\kappa_1\kappa_2}e^{-j\phi_s} & j\sqrt{\kappa_1(1-\kappa_2)}\alpha(V)e^{-j\phi_m(V)} + j\sqrt{(1-\kappa_1)\kappa_2}e^{-j\phi_s}\\ j\sqrt{(1-\kappa_1)\kappa_2}\alpha(V)e^{-j\phi_m(V)} + j\sqrt{\kappa_1(1-\kappa_2)}e^{-j\phi_s} & -\sqrt{\kappa_1\kappa_2}\alpha(V)e^{-j\phi_m(V)} + \sqrt{(1-\kappa_1)(1-\kappa_2)}e^{-j\phi_s}\end{bmatrix}\times\begin{bmatrix}E_{in1}\\E_{in2}\end{bmatrix}\end{aligned} \tag{5}$$

where E_{out1} and E_{out2} are the electrical field of the TC's outputs, E_{in1} and E_{in2} are the inputs' electrical field, κ_1 and κ_2 are the splitting ratios of the TC1 and TC2.

To implement a pure phase modulation, we set $\mathbf{E_{in2}} \equiv \mathbf{0}$ and monitor $\mathbf{E_{out1}}$, which is:

$$\begin{aligned}E_{out1} &= [\sqrt{(1-\kappa_1)(1-\kappa_2)}\alpha(V)e^{-j\phi_m(V)} - \sqrt{\kappa_1\kappa_2}e^{-j\phi_s}]E_{in1}\\ &= [\sqrt{(1-\kappa_1)(1-\kappa_2)}\alpha(V)e^{-j\phi_m(V)} + \sqrt{\kappa_1\kappa_2}e^{-j(\phi_s-\pi)}]E_{in1}\end{aligned} \tag{6}$$

It can be seen that the transmission of the configurable modulator is the sum of two complex phasors, where the PDM rotates one phasor (say, τ_1) and varies its amplitude with the applied modulation signal, and the PS rotates the other phasor (say, τ_2) with applied bias voltage. If a phase shifter with 2π tuning range is used, the angle between τ_1, τ_2 can be arbitrarily set. Because κ_1 and $\kappa_2 \in [0, 1]$, the ratio $\sqrt{\frac{(1-\kappa_1)(1-\kappa_2)}{\kappa_1\kappa_2}}$ can be tuned in $[0, \infty)$, which means that the relative intensity of τ_1, τ_2 can be arbitrarily set.

Adjusting the two phasors' relative intensity and angle can significantly suppress the spurious intensity modulation introduced by the PDM. The principle can be illustrated by phasor diagrams. Figure 3 shows the phase diagrams for a carrier depletion modulator based configurable modulator. The output amplitude is the magnitude of the phasor, while the output phase rotation is indicated by the angle of the phasor. The phasor of the modulator arm τ_1 is drawn in red, while the phasor of the phase shifter arm τ_2 is drawn in blue. The sum of the phasors, corresponding to the output signal, is drawn in green. The relative magnitude and orientation of the red and blue phasor is determined by the κ_1, κ_2 of the TCs and ϕ_S of the static phase shifter. When the carrier depletion modulator is being modulated, the red phasor will move. For instance, with a carrier depletion modulator rotates τ_1 clockwise and increases in amplitude, as shown as the red curve. As a result, the angle between τ_1 and τ_2 changes, which has an effect on the intensity of the sum of the two phasors. When the magnitude and phase of the blue phasor is properly chosen, this effect will compensate the effect of the intensity increase of the carrier depletion modulator in the sum of τ_1 and τ_2, as shown as the green curve. As such, the spurious intensity modulation is suppressed.

The principle for a carrier injection modulator is similar, as shown in Fig. 4. With forward biased PIN junction, the injection modulator rotates τ_1 counterclockwise and reduces its intensity. However, if τ_2 is set as shown in Fig. 4(d), the angle between τ_1 and τ_2 is decreased when τ_1 is rotated. Thus the intensity of the phasor sum is increased, compensating the spurious intensity modulation.

Optics EXPRESS

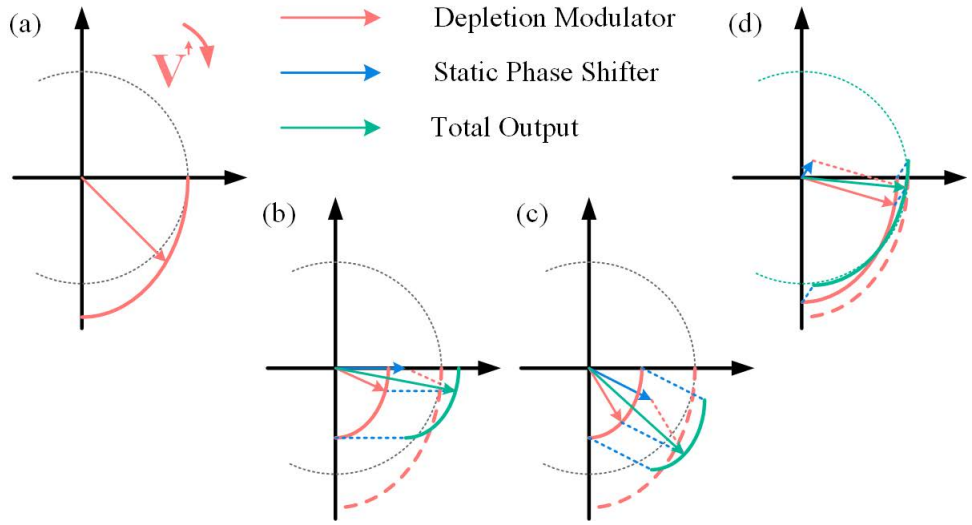

Fig. 3. Phasor diagrams for a carrier depletion modulator based configurable modulator. (a) All light feeds into the depletion modulator; (b) half of the light feeds into the modulator and the other half goes into the phase shifter with zero phase shift; (c) half of the light feeds into the modulator and half goes to the phase shifter with a nonzero phase shift; (d) one of the optimized conditions for pure phase modulation.

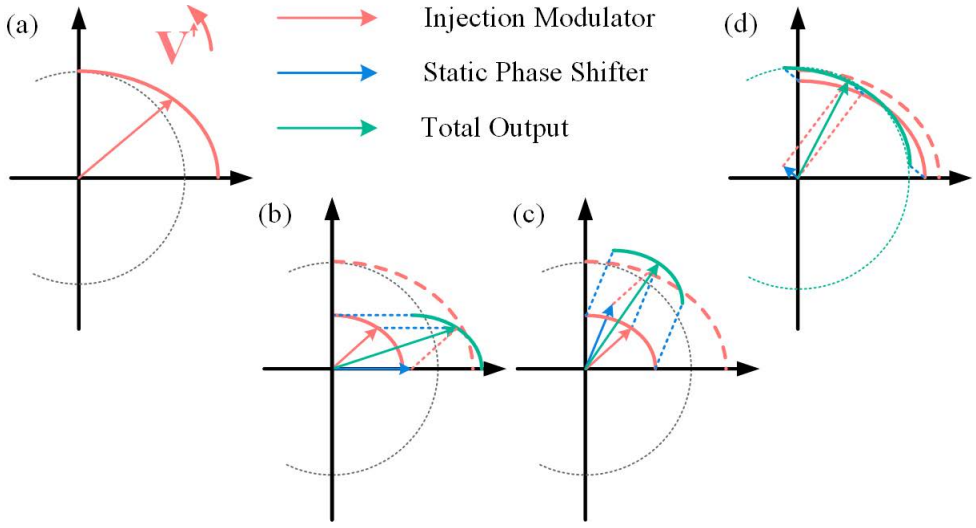

Fig. 4. Phasor diagrams for a carrier injection modulator based configurable modulator. (a) All light feeds into the injection modulator; (b) half of the light feeds into the modulator and the other half goes to the phase shifter with zero phase shift; (c) half of the light feeds into the modulator and half goes to the phase shifter with a nonzero phase shift; (d) one of the optimized conditions.

Optics EXPRESS

3. Simulation and discussion

3.1. Carrier depletion modulator

To implement a simulation, a physical depletion modulator model with 1000 μm length is constructed, and its direct current response is shown in Fig. 1(a) and 1(b) [9]. A direct description between the phase change and the intensity change using a polar diagram is shown in Fig. 1(c), where the radius indicates the intensity on a linear scale and the azimuth shows the phase shifts. As can be seen, for reverse biased voltage from 0 to 6 V, the depletion modulator provides a 0.4 π phase modulation (from 0° to -71.7°) and a 1.26 dB spurious intensity modulation (from 0.75 to 0.87).

From Eq. (6), we can find three degrees of freedom, κ_1, κ_2 and ϕ_s, to minimize the spurious intensity modulation. First we performed a sweeps of κ_1 and κ_2 at fixed ϕ_s. Figure 5(a) and 5(b) show the spurious modulation at $\phi_s = 0$ and $\phi_s = -0.2\pi$. The contour line shows the spurious intensity modulation, where lower values are better. From Fig. 5(a), it can be found that two areas have lower intensity modulation than the other parts. Area 1 is located near $\kappa_1 = 1$ or $\kappa_2 = 1$, where nearly no light is fed to the depletion modulator, which will result in little or no modulation at all. Area 2 is more useful, where κ_1 and κ_2 are somewhat lower than 0.5. Comparing Fig. 5(a) and 5(b), we can find that different ϕ_s lead to different varying range, but the target area still locates at a similar area. In addition, the figures show a symmetry between κ_1 and κ_2, which can be proven by Eq. (6).

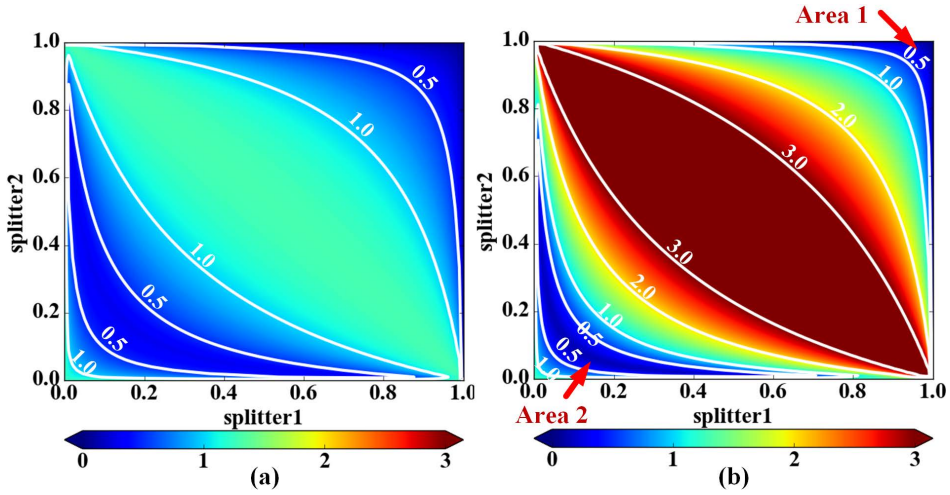

Fig. 5. (a) Spurious intensity modulation with depletion modulator: sweep κ_1 and κ_2 at $\phi_s = 0$; (b) Spurious intensity modulation with depletion modulator: sweep κ_1 and κ_2 at $\phi_s = -0.2\pi$.

this symmetry allows us to set $\kappa = \kappa_1 = \kappa_2$ for the remainder of the discussion and then sweep κ (from 0.02 to 0.49), and ϕ_s (from $-\pi$ to π) to investigate how the spurious intensity modulation changes, and the simulation results are shown in Fig. 6. Again, the contour line shows the spurious intensity modulation. A,B,C,D represent four different operating points and their corresponding polar diagrams. Red curves show the modulation curve of the depletion modulator and the green ones show the modulation curve of the configurable MZI modulator. In a crescent region, the minimum spurious intensity modulation can be suppressed down to 0.023 dB minimally, as shown at the operation point A and in Fig. 8. At point B, the modulation curve shows a large intensity modulation, but with a small phase modulation, turning the configurable modulator into an intensity modulator. At point C, it can be seen that the total insertion loss

Optics EXPRESS

is reduced, but the phase modulation range is also significantly suppressed. At point D, the modulation curve is close to the zero point, and phase modulation of more than π phase range is achieved, which makes the modulator suitable for binary π phase modulation.

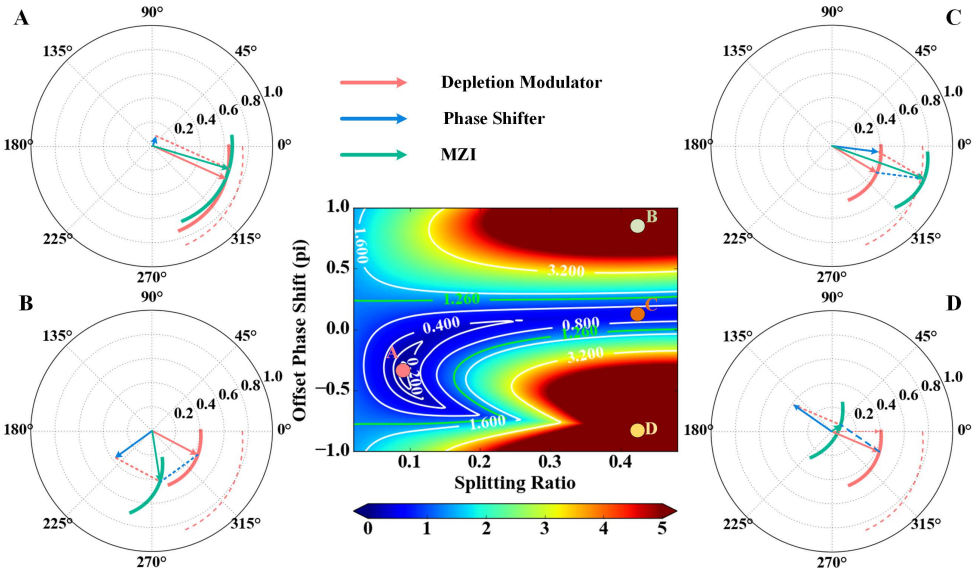

Fig. 6. Simulation results with depletion modulator for minimal spurious intensity modulation: sweep splitting ratio and offset phase shifts. Operation points: A: $\kappa = 0.092$ and $\phi_s = -0.384\pi$; B: $\kappa = 0.42$ and $\phi_s = 0.8\pi$; C: $\kappa = 0.42$ and $\phi_s = 0.05\pi$; D: $\kappa = 0.42$ and $\phi_s = -0.8\pi$.

From Fig. 6, it can be seen that different operation points lead to different phase modulation ranges, optical losses, and nonlinearities. The other performance metrics which are indicated in Fig. 1 are plotted in Fig. 7. Figure 7(a) shows the spurious intensity modulation as shown in Fig. 6. Figure 7(b) indicates the nonlinearity of the phase modulation, which is defined by the maximum phase deviation from a fitted straight line over the phase modulation range, and it should be as low as possible for many microwave photonic applications. Figure 7(c) expresses the minimum intensity (i.e the lowest optical transmission during modulation), which should be as high as possible. Figure 7(d) elaborates the phase modulation range. In addition, the green curves in those figures are the characteristics of the bare depletion modulator model that we used, which are 1.26 dB intensity modulation, 0.058 nonlinearity, 0.750 minimum intensity and 0.398 π phase modulation. According to Fig. 7, we can determine the operation point to implement a phase modulator with required performance.

The green curve in Fig. 8 shows a modulation curve for pure phase modulation (as operation point A in Fig. 6), with a intensity modulation of 0.02 dB, 0.040 nonlinearity, a phase modulation range of 0.41 π and 1 dB extra optical loss. If a large modulation range is needed, several of these configurable modulator circuits can be cascaded to achieve a larger modulation range with a low spurious intensity modulation. These cascaded modulators can be driven from the same high-speed signal, not complicating the electrical control.

3.2. *Carrier injection modulator*

For the modelling of an injection modulator, we measured a device with a length of 500 μm. The measured direct current responses for intensity and phase are shown in Fig. 1(d) and 1(e), and the modulation curve in polar diagram is shown in Fig. 1(f). Because the PIN junction varies

Optics EXPRESS

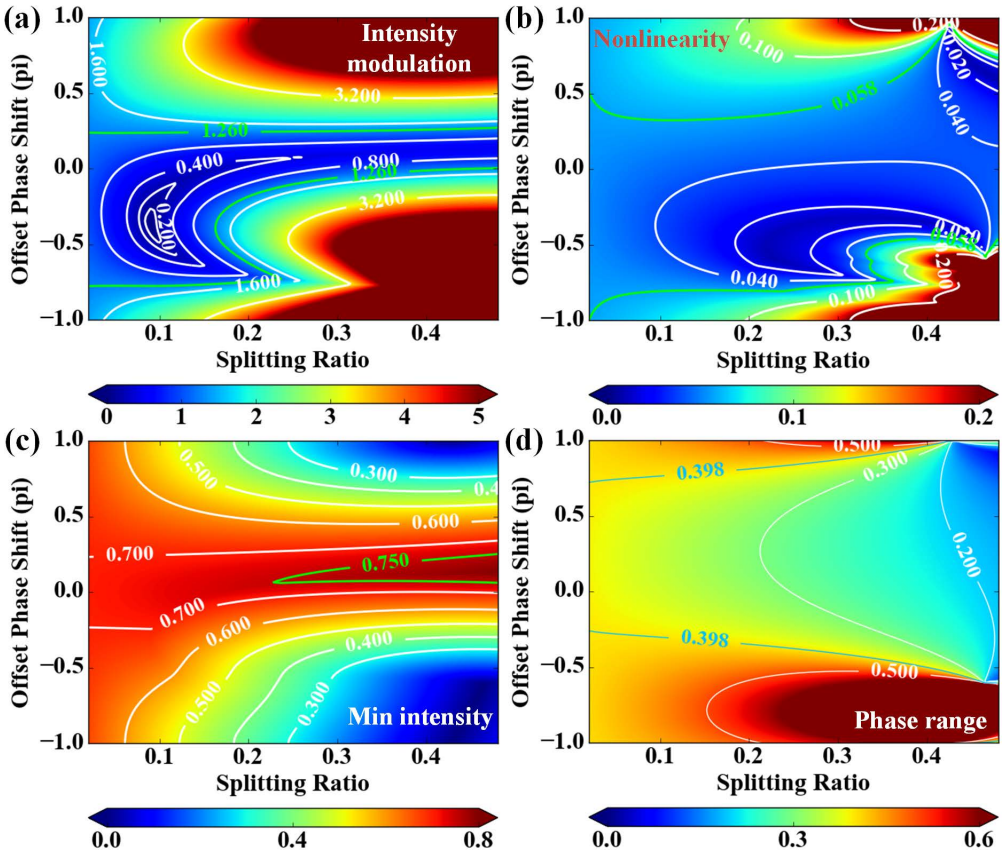

Fig. 7. Simulation results with depletion modulator within 0 V to 6 V. (a) spurious intensity modulation; (b) nonlinearity of phase modulation; (c) minimal intensity; (d) phase modulation range. Green curve show the performance of the used depletion modulator.

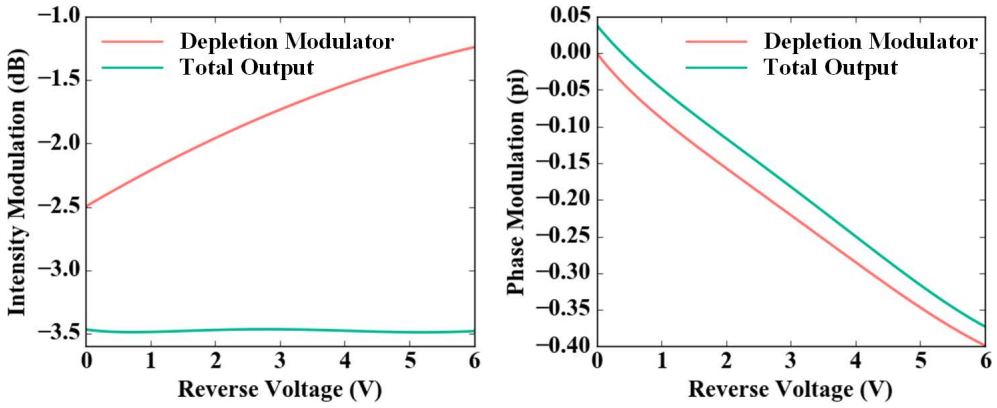

Fig. 8. DC response of a depletion modulator (blue) and the configurable MZI modulator working at $\kappa_1 = \kappa_2 = 0.092$ and $\phi_s = -0.384\pi$ (green).

Optics EXPRESS

dramatically with the forward biased voltage, we limited the voltage range from 0.8 V to 0.9 V, with a spurious intensity modulation of 1.27 dB and a phase modulation range of 0.75 π. Following the simulation steps described above, we can get the simulation results shown in Fig. 9.

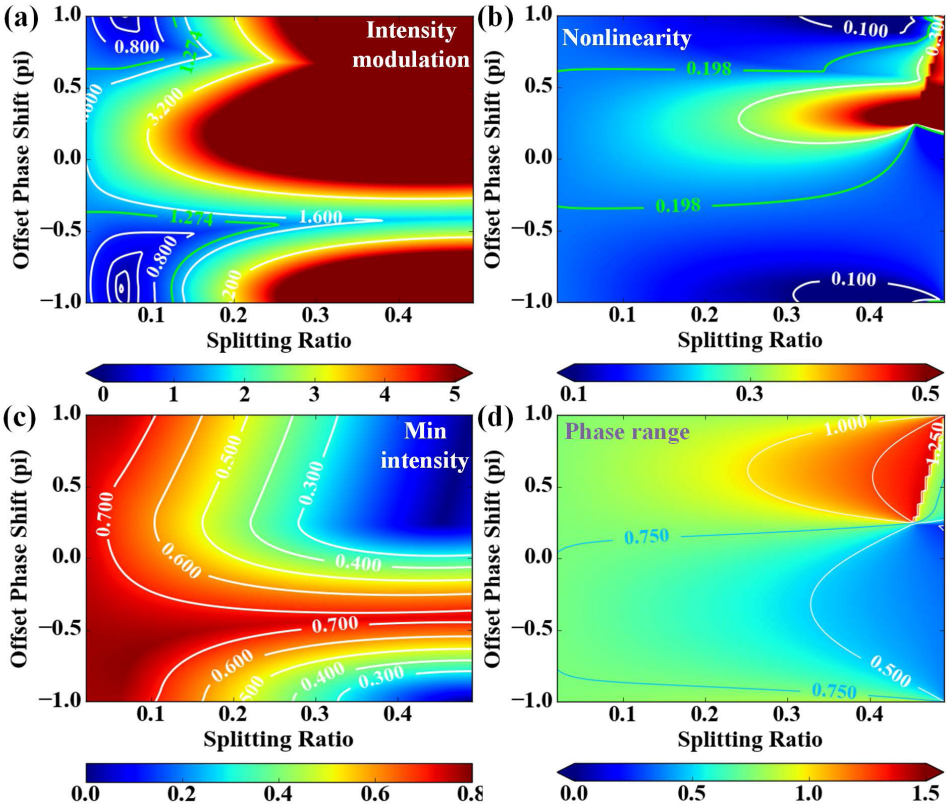

Fig. 9. Simulation results with injection modulator within 0.8 V to 0.9 V. (a) spurious intensity modulation; (b) nonlinearity of phase modulation; (c) minimal intensity; (d) phase modulation range. Green curve show the performance of the used injection modulator.

Also, according to Fig. 9 we can determine the best operation point. Figure 10 shows a modulation curve for pure phase modulation, with an intensity modulation of 0.07 dB, a phase modulation range of 0.76 π and an extra 0.5 dB optical loss.

It should be noted that the spurious intensity modulation cannot be suppressed efficiently when the phase modulation range of the proposed configurable modulator becomes too large, which depends on the modulation curve of the used PDM. If a smaller voltage range is selected, a better performance can be achieved, which is a trade-off. Figure 11(a) shows the achievable lowest spurious intensity modulation with the injection modulator model at different voltages and Fig. 11(b) shows the corresponding phase modulation range. It can be seen that, the optimized configurable modulator has a similar phase modulation range as the injection modulator, while its spurious intensity modulation goes up rapidly when the phase range exceeds π. When the injection modulator provides a 2π phase range (0.8 V to 0.953 V), the optimization can only provide a 0.28 dB suppression on spurious intensity modulation. Again, a larger modulation range can be achieved by cascading several configurable modulators, with a low spurious intensity modulation.

Optics EXPRESS

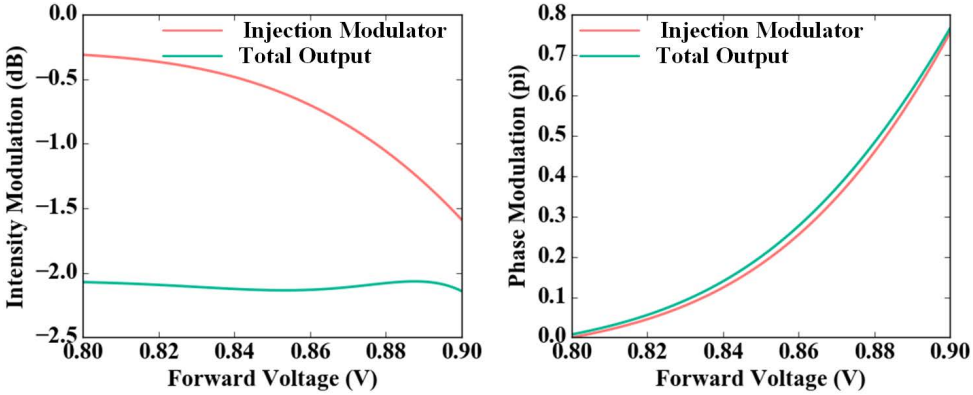

Fig. 10. Pure phase modulation based on an injection modulator. $\kappa_1 = \kappa_2 = 0.063$ and $\phi_s = -0.9\pi$.

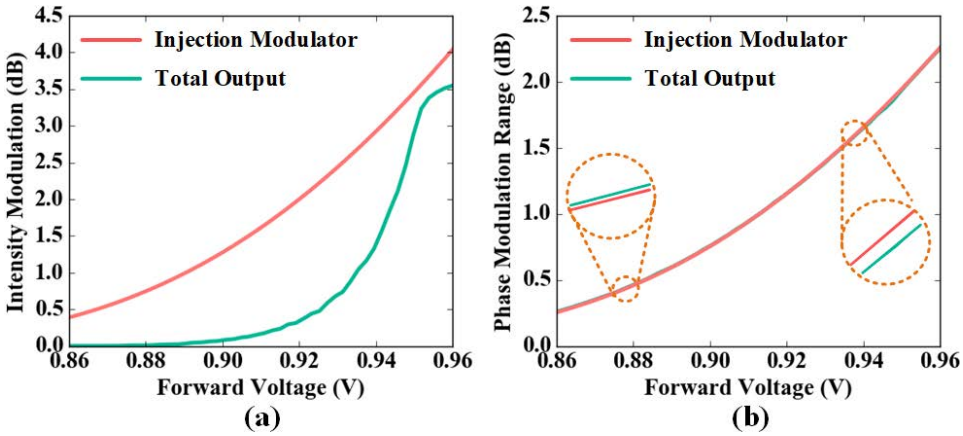

Fig. 11. (a)Minimal intensity modulation and (b) phase modulation range for the injection modulator and the optimized configurable modulator at different voltage ranges (0.8 V to Max voltage).

4. Conclusion

In this article, we proposed a method to realize pure phase modulation using an unmodified silicon plasma dispersion modulators, by embedding them in a configurable modulator MZI circuit. By tuning the coupling ratios of the TCs and the phase delay between the two arms of the MZI, the spurious intensity modulation introduced by the PDM can be suppressed. We explored this behaviour in simulation for both depletion modulators and injection modulators. Simulation results show that, for depletion modulator, the 1.26 dB spurious intensity modulation can be suppressed down to 0.023 dB within a phase range of 0.4π, and for injection modulator, the 1.27 dB spurious intensity modulation can be suppressed down to 0.07 dB within a phase range of 0.75π. In addition, the trade-off among spurious intensity modulation, modulation range, linearity and optical loss of a phase modulator was discussed.

Funding

H2020 European Research Council (725555).

Optics EXPRESS

References

1. W. Bogaerts and L. Chrostowski, "Silicon Photonics Circuit Design: Methods, Tools and Challenges," Laser Photonics Rev. **12**(4), 1700237 (2018).
2. Y. Shen, X. Meng, Q. Cheng, S. Rumley, N. Abrams, A. Gazman, E. Manzhosov, M. Strom Glick, and K. Bergman, "Silicon Photonics for Extreme Scale Systems," J. Lightwave Technol. **37**(2), 245–259 (2019).
3. H. Deng, P. Lu, S. J. Mihailov, and J. Yao, "High-Speed and High-Resolution Interrogation of a Strain and Temperature Random Grating Sensor," J. Lightwave Technol. **36**(23), 5587–5592 (2018).
4. D. Marpaung, J. Yao, and J. Capmany, "Integrated microwave photonics," Nat. Photonics **13**(2), 80–90 (2019).
5. J. Witzens, "High-Speed Silicon Photonics Modulators," Proc. IEEE **106**(12), 2158–2182 (2018).
6. W. Bogaerts, P. D. Heyn, T. V. Vaerenbergh, K. D. Vos, S. K. Selvaraja, T. Claes, P. Dumon, P. Bienstman, D. V. Thourhout, and R. Baets, "Silicon microring resonators," Laser Photonics Rev. **6**(1), 47–73 (2012).
7. R. Soref and B. Bennett, "Electrooptical effects in silicon," IEEE J. Quantum Electron. **23**(1), 123–129 (1987).
8. M. Nedeljkovic, R. Soref, and G. Z. Mashanovich, "Free-carrier electrorefraction and electroabsorption modulation predictions for silicon over the 1-14-μm infrared wavelength range," IEEE Photonics J. **3**(6), 1171–1180 (2011).
9. H. Yu, M. Pantouvaki, J. V. Campenhout, D. Korn, K. Komorowska, P. Dumon, Y. Li, P. Verheyen, P. Absil, L. Alloatti, D. Hillerkuss, J. Leuthold, R. Baets, and W. Bogaerts, "Performance tradeoff between lateral and interdigitated doping patterns for high speed carrier-depletion based silicon modulators," Opt. Express **20**(12), 12926 (2012).
10. M. Lauermann, R. Palmer, S. Koeber, P. C. Schindler, D. Korn, T. Wahlbrink, J. Bolten, M. Waldow, D. L. Elder, L. R. Dalton, J. Leuthold, W. Freude, and C. Koos, "Low-power silicon-organic hybrid (SOH) modulators for advanced modulation formats," Opt. Express **22**(24), 29927 (2014).
11. N. C. Harris, Y. Ma, J. Mower, T. Baehr-Jones, D. Englund, M. Hochberg, and C. Galland, "Efficient, compact and low loss thermo-optic phase shifter in silicon," Opt. Express **22**(9), 10487 (2014).
12. A. Liu, L. Liao, D. Rubin, H. Nguyen, B. Ciftcioglu, Y. Chetrit, N. Izhaky, and M. Paniccia, "High-speed optical modulation based on carrier depletion in a silicon waveguide," Opt. Express **15**(2), 660 (2007).
13. D. Patel, S. Ghosh, M. Chagnon, A. Samani, V. Veerasubramanian, M. Osman, and D. V. Plant, "Design, analysis, and transmission system performance of a 41 GHz silicon photonic modulator," Opt. Express **23**(11), 14263 (2015).
14. Z. Wang, Y. Gao, A. S. Kashi, J. C. Cartledge, and A. P. Knights, "Silicon Microring Modulator for Dispersion Uncompensated Transmission Applications," J. Lightwave Technol. **34**(16), 3675–3681 (2016).
15. A. Ribeiro, W. Bogaerts, M. Nedeljkovic, Y. Hu, D. J. Thomson, K. Li, P. R. Wilson, S. Chen, and S. S. Hsu, "Digitally controlled multiplexed silicon photonics phase shifter using heaters with integrated diodes," Opt. Express **25**(24), 29778 (2017).
16. Y. Xing, T. Ako, J. P. George, D. Korn, H. Yu, P. Verheyen, M. Pantouvaki, G. Lepage, P. Absil, A. Ruocco, C. Koos, J. Leuthold, K. Neyts, J. Beeckman, and W. Bogaerts, "Digitally controlled phase shifter using an SOI slot waveguide with liquid crystal infiltration," IEEE Photonics Technol. Lett. **27**(12), 1269–1272 (2015).
17. K. Suzuki, G. Cong, K. Tanizawa, S.-H. Kim, K. Ikeda, S. Namiki, and H. Kawashima, "Ultra-high-extinction-ratio 2 × 2 silicon optical switch with variable splitter," Opt. Express **23**(7), 9086 (2015).